The Astronomical Journal, 136:2453–2467, 2008 December doi:10.1088/0004-6256/136/6/2453

STABILITY OF THE DISTANT SATELLITES OF THE GIANT PLANETS IN THE SOLAR SYSTEM

Yue Shen[1] and Scott Tremaine[2]
[1] Princeton University Observatory, Princeton, NJ 08544, USA
[2] Institute for Advanced Study, Princeton, NJ 08540, USA
Received 2008 June 17; accepted 2008 September 16; published 2008 November 13

ABSTRACT

We conduct a systematic survey of the regions in which distant satellites can orbit stably around the four giant planets in the solar system, using orbital integrations of up to 10^9 yr. In contrast to previous investigations, we use a grid of initial conditions on a surface of section to explore phase space uniformly inside and outside the planet's Hill sphere (radius $r_{\rm H}$; satellites outside the Hill sphere sometimes are also known as quasi-satellites). Our confirmations and extensions of old results and new findings include the following: (1) many prograde and retrograde satellites can survive out to radii $\sim 0.5 r_{\rm H}$ and $\sim 0.7 r_{\rm H}$, respectively, while some coplanar retrograde satellites of Jupiter and Neptune can survive out to $\sim r_{\rm H}$; (2) stable orbits do not exist within the Hill sphere at high ecliptic inclinations when the semimajor axis is large enough that the solar tide is the dominant non-Keplerian perturbation; (3) there is a gap between $\sim r_{\rm H}$ and $2r_{\rm H}$ in which no stable orbits exist; (4) at distances $\gtrsim 2r_{\rm H}$ stable satellite orbits exist around Jupiter, Uranus, and Neptune (but not Saturn). For Uranus and Neptune, in particular, stable orbits are found at distances as large as $\sim 10 r_{\rm H}$; (5) the differences in the stable zones beyond the Hill sphere arise mainly from differences in the planet/Sun mass ratio and perturbations from other planets; in particular, the absence of stable satellites around Saturn is mainly due to perturbations from Jupiter. It is, therefore, likely that satellites at distances $\gtrsim 2r_{\rm H}$ could survive for the lifetime of the solar system around Uranus, Neptune, and, perhaps, Jupiter.

Key words: celestial mechanics – minor planets, asteroids – planets and satellites: formation – planets and satellites: general

Online-only material: color figures

1. INTRODUCTION

Most of the satellites of the four giant planets in the solar system can be divided into two groups, usually called the regular and irregular satellites. Regular satellites orbit close to the planet (within $\sim 0.05 r_{\rm H}$, where $r_{\rm H}$ is the Hill radius[3]), and move on nearly circular, prograde orbits that lie close to the planetary equator. Irregular satellites are found at distances $\sim 0.05 r_{\rm H}$–$0.6 r_{\rm H}$, with large orbital eccentricities and inclinations, on both prograde and retrograde orbits. An alternative division between regular and irregular satellites is given by the critical semimajor axis (e.g., Goldreich 1966; Burns 1986), $a_{\rm crit} = \left(2\mu J_2 R^2 a_p^3\right)^{1/5}$; those with $a > a_{\rm crit}$ are classified as irregular satellites. Here J_2 is the planet's second zonal harmonic coefficient (augmented by any contribution from the inner regular satellites) and R is the planet's radius. This critical radius marks the location where the precession of the satellite's orbital plane is dominated by the Sun rather than by the planet's oblateness. The current number ratios of irregular to regular satellites are 55/8 for Jupiter, 35/21 for Saturn, 9/18 for Uranus, and 7/6 for Neptune (e.g., Jewitt & Haghighipour 2007). The regular satellites are likely to have formed within a circumplanetary disk of gas and solid bodies. The kinematic differences between regular and irregular satellites suggest that the latter must have formed through a quite different mechanism, most likely capture from the circumstellar disk (for a recent review, see Jewitt & Haghighipour 2007).

The search for irregular satellites of the giant planets has been fruitful in recent years, owing mainly to modern high-sensitivity, large-scale CCDs (e.g., Gladman et al. 1998, 2000, 2001; Holman et al. 2004; Kavelaars et al. 2004; Sheppard & Jewitt 2003; Sheppard et al. 2005, 2006). By 2007, 106 irregular satellites of the giant planets had been discovered, compared with 53 regular satellites. Two features stand out in the distributions of orbital parameters of these irregular satellites. First, retrograde irregular satellites extend to larger semimajor axes than prograde ones ($\sim 0.6 r_{\rm H}$ compared to $\sim 0.4 r_{\rm H}$); second, satellites with orbital inclination in the range $\sim 60^\circ$–130° relative to the ecliptic are absent.

A number of authors have shown that these features can be explained reasonably well by the requirement that the satellite orbits be stable. Hénon (1969, 1970) studied the planar circular restricted three-body problem in Hill's (1886) approximation, where the mass ratio $\mu \to 0$ while the radii of interest shrink to zero as $\mu^{1/3}$. He showed that prograde satellite orbits are stable up to a mean distance from the planet $\sim 0.4 r_{\rm H}$, while retrograde satellite orbits can be stable at much larger distances from the planet. Thus, it is not surprising that retrograde satellites are found at larger distances than prograde ones. Hamilton & Krivov (1997) studied the dynamics of distant satellites of asteroids in heliocentric orbits using a "generalized Tisserand constant" and, among other conclusions, confirmed that retrograde orbits are more stable than prograde ones. Carruba et al. (2002) used a combination of analytic arguments and numerical integrations to show that high-inclination orbits inside the Hill sphere exhibit large eccentricity oscillations (Kozai oscillations; Kozai 1962) due to secular solar perturbations. They found that orbits with inclinations (relative to the planetary orbital plane) between 55° and 130° are generally unstable, thus explaining the absence of irregular satellites on high-inclination orbits. Nesvorný et al. (2003) performed detailed orbital integrations of the four giant planets plus a grid of test-particle satellites for intervals of 10^6–10^8 yr. They confirmed that retrograde satellites can be stable at

[3] The Hill radius is defined as $r_{\rm H} = a_p(\mu/3)^{1/3}$, where a_p is the semimajor axis of the planet orbit and $\mu \equiv m_p/(m_p + M_\odot)$ with m_p being the planet mass.

larger radii than prograde ones, and that highly inclined orbits are unstable. They argued that the largest semimajor axes at which satellites of the four giant planets could survive for times comparable to the lifetime of the solar system were $\sim 0.7 r_{\rm H}$ for retrograde satellites and $\sim 0.4 r_{\rm H}$ for prograde ones, and that these upper limits were achieved only for nearly circular orbits close to the plane of the ecliptic.

Other authors have examined the possibility that stable satellite orbits exist with mean distance from the planet $\gtrsim r_{\rm H}$. In the planetocentric frame, the dominant force on such satellites is due to the Sun, rather than the planet.[4] Nevertheless, the satellite remains close to the planet because it is in a 1:1 resonance in the sense that its heliocentric mean longitude librates around that of the planet; the resulting orbit relative to the planet is a retrograde ellipse with an axis ratio of 2:1 with the short axis pointing toward the Sun, and synodic period equal to the planet's orbital period. The analytical theory of such orbits is described by Jackson (1913), Lidov & Vashkov'yak (1994a, 1994b), Mikkola & Innanen (1997), Namouni (1999), Mikkola et al. (2006), and others. Hénon's (1970) numerical analysis of Hill's approximation to the planar circular restricted three-body problem suggests that stable retrograde satellites can exist at arbitrarily large distance from the planet. Benest (1971) confirmed that stable retrograde orbits at large distances persist in the elliptic restricted three-body problem, where the mass ratio and eccentricity were chosen to match those of Jupiter. Wiegert et al. (2000) demonstrated that the retrograde satellites of Uranus and Neptune could be stable for up to 10^9 yr at distances up to $\sim 10 r_{\rm H}$, suggesting that primordial objects of this type could still exist in the solar system although none are currently known.

Despite the number and quality of these investigations, there are several unanswered questions that lead us to revisit the problem of orbital stability of satellites at large distances from the host planet.

1. Wiegert et al. (2000) found stable satellite orbits beyond the Hill radius only for Uranus and Neptune, not Jupiter or Saturn. What is the reason for this difference? The possibilities include differences in the planetary masses and orbital eccentricities, or different perturbations from neighboring planets.
2. Wiegert et al. (2000) explored orbits outside the Hill radius, while Nesvorný et al. (2003) explored orbits inside the Hill radius (indeed, in the former paper the integrations were terminated when the particles entered the Hill sphere of radius $r_{\rm H}$ around the planet, while in the latter paper the integrations were terminated when the particles exited The Hill sphere). Are there stable satellite orbits that cross the Hill sphere?
3. As we shall describe further in Section 2, the grids of initial conditions used by Nesvorný et al. and Wiegert et al. do not provide a complete exploration of the phase space in which stable satellite orbits exist.

The primary goal of this paper is to map out the entire stability region in phase space—both inside and outside the Hill sphere—in which satellite orbits can survive around the four giant planets for times comparable to the age of the solar system (our main integrations last for up to 100 Myr). We describe our setup in Section 2, and present the results in Section 3. We conclude and discuss our results in Section 4.

Following Fabrycky (2008), we shall define a "satellite" of a planet to be a small body whose distance from the planet never exceeds the semimajor axis of the planet, a_p. This definition excludes bodies on Trojan orbits around the triangular Lagrange points, bodies on horseshoe orbits, and objects such as asteroid 2003 YN107 (Connors et al. 2004), which oscillates between a horseshoe orbit and an orbit centered on the Earth. This definition seems simple and reasonable to us, but other definitions are common in the literature. Many authors define "satellite" to be an object that always remains within the Hill sphere of the planet or whose Jacobi constant constrains it to remain within the last closed zero-velocity surface around the planet. Benest (1971) defines a satellite to be a body whose heliocentric orbital frequency is the same as the planet's, but whose synodic frequency around the planet is nonzero. Wiegert et al. (2000) use the term "quasi-satellite" for an object that remains outside the Hill sphere but whose heliocentric longitude difference from the planet never exceeds 120° and regularly passes through zero. However, the term "quasi-satellite" is confusing because it is also used for objects such as 2003 YN107 that spend part of their time on horseshoe orbits, and thus are only temporarily satellites in our sense.

2. METHODS

Although all of our results are based on direct numerical integrations of the N-body problem (the Sun, one or four giant planets, plus a test particle orbiting one planet), we shall find it useful to interpret our results in terms of the coordinates and notation used by Hénon (1970) in the exploration of satellite orbits in Hill's approximation.

2.1. Hill's Approximation

When studying satellite motions near a planet ($r \ll r_{\rm H}$), it is conventional to employ a *nonrotating* planetocentric coordinate system, which we denote as (xyz). However, in Hill's approximation to the circular restricted three-body problem, it is more convenient to use a *rotating* planetocentric coordinate system $(\xi\eta\zeta)$, where ξ, η, and ζ are scaled coordinates in the rotating frame in which the planet is at the origin, the ξ axis is along the direction opposite the Sun, and the ζ axis is perpendicular to the Sun–planet orbital plane. In Hill's formulation the unit of length is $\mu^{1/3} a_p$, and the unit of time is n^{-1}, where $n \equiv \left[G(M_\odot + m_p)/a_p^3\right]^{1/2}$ is the mean motion of the planet. As usual, the orbit of the planet in the inertial frame is counterclockwise as viewed from the positive z or ζ axis. In Hill's coordinate system the collinear Lagrangian points L_1 and L_2 are located at $\eta = \zeta = 0, \xi = \pm 3^{-1/3} \simeq 0.6934$, and the Hill radius is $r_{\rm H} = 3^{-1/3}$. Similar definitions are used in this paper when the planet orbit is eccentric and/or perturbed by other planets; in this case, the ξ axis points away from the instantaneous position of the Sun, the ζ axis is perpendicular to the instantaneous orbital plane of the planet around the Sun, and a_p is the initial semimajor axis of the planet.

In the circular restricted three-body problem, Hill's approximation is achieved by taking the limit $\mu \to 0$, where the equations of motion reduce to (e.g., Hénon 1974; Murray & Dermott 1999)

$$\ddot{\xi} = 2\dot{\eta} + 3\xi - \frac{\xi}{(\xi^2+\eta^2+\zeta^2)^{3/2}},$$
$$\ddot{\eta} = -2\dot{\xi} - \frac{\eta}{(\xi^2+\eta^2+\zeta^2)^{3/2}},$$
$$\ddot{\zeta} = -\zeta - \frac{\zeta}{(\xi^2+\eta^2+\zeta^2)^{3/2}}. \quad (1)$$

[4] Hence these are sometimes called "quasi-satellites" (Lidov & Vashkov'yak 1994a, 1994b; Mikkola & Innanen 1997).

There exists an integral of motion for these equations,

$$\Gamma = 3\xi^2 + \frac{2}{(\xi^2+\eta^2+\zeta^2)^{1/2}} - \zeta^2 - (\dot{\xi}^2+\dot{\eta}^2+\dot{\zeta}^2)\,, \qquad (2)$$

which corresponds to the Jacobi constant in the circular restricted three-body problem.

For the moment let us restrict ourselves to motion in the Sun–planet orbital plane, so $\zeta = \dot{\zeta} = 0$ at all times. Then to study orbital motions we may use a surface of section defined by $\eta = 0, \dot{\eta} > 0$. The trajectory in the four-dimensional $(\xi, \eta, \dot{\xi}, \dot{\eta})$ phase space is then represented by a set of points in the $(\xi, \dot{\xi})$ plane, and for a given value of the Jacobi constant Γ, the other two phase-space coordinates can be derived from

$$\eta = 0, \qquad \dot{\eta} = \left(3\xi^2 - \dot{\xi}^2 + \frac{2}{|\xi|} - \Gamma\right)^{1/2}. \qquad (3)$$

We define "prograde" and "retrograde" in the rotating frame unless otherwise noted. Thus retrograde orbits have $\xi < 0$ in this surface of section, and prograde orbits have $\xi > 0$.

A drawback of this surface of section is that a different plot is needed for each value of the Jacobi constant Γ. To obtain a global view of the dynamics, we use a different surface of section defined by $\eta = 0, \dot{\xi} = 0, \dot{\eta} = (3\xi^2 + 2/|\xi| - \Gamma)^{1/2}$. A trajectory is represented by a point in the (Γ, ξ) plane. This surface of section was introduced by Hénon (1969; 1970), and we shall call it the Hénon surface of section or Hénon diagram. The Hénon diagram, like any surface of section, will not show orbits that do not cross it; the usefulness of the Hénon diagram derives from the observation that most stable orbits periodically pass close to the point $\eta = \dot{\xi} = 0$—for example, this occurs for nearly Keplerian orbits close to the planet when their line of apsides precesses past the Sun–planet line. The orbits not shown on the Hénon diagram include those confined to some resonant islands, which should occupy a small fraction of phase space, and escape orbits, which we are not interested in anyway.

Figure 1 (left panel) is a Hénon diagram modeled on Figure 12 of Hénon (1970). The Lagrange points are at $(\Gamma, \xi) = (3^{4/3}, \pm 3^{-1/3}) = (4.32675, \pm 0.69336)$. Forbidden regions, in which $\dot{\eta}^2 = 3\xi^2 + 2/|\xi| - \Gamma$ would be negative, are shaded in gray. The stable regions of phase space, as estimated by Hénon, are denoted by vertical stripes. The diagram shows that retrograde satellites ($\xi < 0$) have a larger stable region than prograde satellites ($\xi > 0$), a conclusion consistent with the numerical studies described in Section 1. Moreover, the stable band in this diagram that begins at $(\Gamma, \xi) = (-1.4, -1.2)$, and stretches downward to the left shows that retrograde satellites can be stable at distances much larger than the Hill radius; in fact, this band continues to arbitrarily large negative values of Γ and ξ (see Figure 13 of Hénon 1970), so retrograde satellites can be stable at arbitrarily large distances from the planet, at least in Hill's approximation to the planar circular restricted three-body problem.

In future discussions we divide the stable regions in Figure 1 into three branches: the inner prograde branch ($\xi > 0$), the inner retrograde branch ($\xi < 0$ and $\Gamma > 0$), and the outer retrograde branch ($\xi < 0$ and $\Gamma < 0$).

A simple and rather complete way to sample initial conditions in the planar three-body problem is to use the Hénon diagram, i.e., to sample uniformly in the (Γ, ξ) plane. As described above, this approach is based on the assumption that most stable orbits periodically have their apocenter or pericenter on the Sun–planet line. Note that, even without invoking Hill's approximation, the question of which initial conditions on the Hénon diagram correspond to stable orbits is well-posed. Accordingly, we may present our stability results in terms of the Hénon diagrams, even though our orbit integrations do not use Hill's approximation.

We may compare this approach to the grids of initial conditions used in other investigations of the stability of satellite orbits. The initial conditions for the "high-resolution survey" of Nesvorný et al. (2003) were chosen from a grid of planet-centered osculating Keplerian orbital elements, with the semimajor axis a given typically by $a/r_H = 0.1$–1, eccentricity $e = 0$–0.75, inclination $i = 0°$–$180°$, argument of pericenter $\omega = 0°, 90°$, and the other elements distributed uniformly between $0°$ and $360°$. The right panel of Figure 1 shows similar initial conditions on the Hénon diagram ($i = 0°$ or $180°$ and $\omega = 0°$ or $180°$). The conversions from osculating elements to (Γ, ξ) were done using Equations (8) and (10) in Hénon (1970). It is clear that the initial conditions sampled in Nesvorný et al. do not provide a complete exploration of the phase space in which stable satellite orbits could exist; in particular, they completely missed the stable region that extends beyond the Hill sphere (of course, such orbits are also excluded from their study by their artificially imposed escape criterion $r > r_H$). In fact, most of the stable orbits beyond the Hill sphere have hyperbolic osculating elements. In Figure 1 we plot the boundaries that separate regions of hyperbolic osculating elements from those with elliptical osculating elements, where the latter are shaded by a dotted pattern. The functional forms of these boundaries are

$$\Gamma = 2\xi^2 - 2^{3/2}|\xi|^{1/2}\,, \qquad (\xi < 0)\,, \qquad (4)$$

$$\Gamma = 2\xi^2 + 2^{3/2}|\xi|^{1/2}\,, \qquad (0 \leqslant \xi \leqslant 2^{1/3})\,, \qquad (5)$$

$$\Gamma = 2\xi^2 + 2^{3/2}|\xi|^{1/2}\,, \qquad (\xi < -2^{1/3})\,. \qquad (6)$$

The initial conditions explored by Wiegert et al. (2000) were chosen from a grid of heliocentric osculating Keplerian elements, these being the same as the elements of the host planets except for the eccentricity and inclination. The eccentricity was typically chosen in the range $e = 0$–0.5 and inclination in the range $0°$–$30°$. With this procedure, zero-inclination orbits appear in the Hénon diagram along the locus

$$\Gamma = 2/|\xi| - \xi^2 \qquad \text{with} \qquad \xi = -e\mu^{-1/3}\,, \qquad (7)$$

where the expression for Γ is evaluated using Hill's approximation. The grid sampled by Wiegert et al. for $i = 0$ is also shown in the right panel of Figure 1, converted from the heliocentric frame using Hill's units (but without Hill's approximation); for clarity, only Jupiter and Uranus are shown. Although the initial conditions of Wiegert et al. do probe the stability region found by Hénon beyond the Hill sphere, the coverage is far from complete.

To extend our study to three-dimensional orbital motions we use a surface of section at $\eta = \zeta = \dot{\xi} = 0, \dot{\eta} > 0$. In the rotating frame, we define the initial inclination angle I by

$$\tan I = \left.\frac{\dot{\zeta}}{\dot{\eta}}\right|_{t=0}\,, \qquad (8)$$

such that the initial η and ζ component velocities are

$$\dot{\eta} = \cos I\left(3\xi^2 + \frac{2}{|\xi|} - \Gamma\right)^{1/2}, \quad \dot{\zeta} = \sin I\left(3\xi^2 + \frac{2}{|\xi|} - \Gamma\right)^{1/2}. \qquad (9)$$

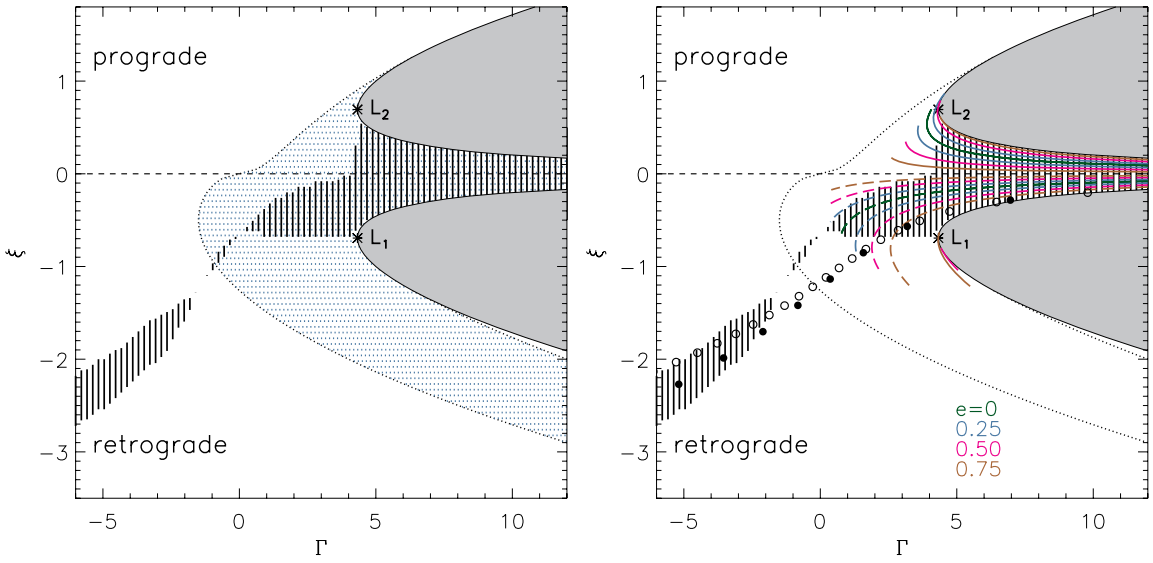

Figure 1. Sampling of initial conditions in terms of the Hénon diagram. The gray-shaded regions are forbidden. The Lagrange points L_1 and L_2 are marked by $*$. The horizontal dashed line at $\xi = 0$ separates retrograde orbits from prograde ones (as defined in the rotating planetocentric frame). Left: the region shaded by vertical lines is an approximate reproduction of the stable region as estimated in Hénon (1970). The dotted region is where the osculating Kepler elements correspond to bound elliptical orbits ($a > 0$, $e < 1$). Right: curved lines represent the initial conditions derived using osculating elements in the high-resolution survey of Nesvorný et al. (2003), color-coded according to eccentricity. Solid and long-dashed lines represent orbits which are prograde and retrograde in the *nonrotating* planetocentric frame, respectively. There are two sets of lines for each eccentricity corresponding to argument of pericenter $\omega = 0°$ and 180°, respectively. The short segments at the lower right below L_1 are extensions of the $e = 0.50$ and 0.75 branches which are prograde in the nonrotating frame. Thus orbits that are retrograde in the rotating frame can be prograde in the nonrotating frame. The initial conditions for zero-inclination orbits sampled by Wiegert et al. (2000) are shown as filled circles for Uranus and open circles for Jupiter.

(A color version of this figure is available in the online journal.)

Since $\dot{\eta} > 0$, the inclination is restricted to the range $-90° < I < 90°$.

Therefore each point in the (Γ, ξ) plane represents a unique set of initial conditions for a given inclination. The usefulness of the Hénon diagram, in this case, is based on the assumption that most stable orbits periodically have their line of apsides and their line of nodes simultaneously on the Sun–planet line. This assumption is not always valid: it requires that the argument of pericenter ω is periodically 0 or π, while a satellite trapped in the Kozai resonance has an argument of pericenter that librates around $\frac{1}{2}\pi$ or $\frac{3}{2}\pi$ (Kozai 1962; Carruba et al. 2002). We estimate the incompleteness in our survey due to such orbits in Section 3.2.

Because the equations of motion are symmetric around the $\zeta = 0$ plane, we may further restrict the inclination to the range $0° \leqslant I < 90°$. As in the two-dimensional case, we define "prograde" and "retrograde" in the rotating frame unless otherwise noted. Thus retrograde orbits have $\xi < 0$ and prograde orbits have $\xi > 0$ at this surface of section $\eta = \zeta = \dot{\xi} = 0$, $\dot{\eta} > 0$.

2.2. Numerical Orbit Integrations

Even in the two-dimensional case, we expect that the stable regions for distant satellites of the giant planets will be somewhat different from those derived by Hénon (1970) and shown in Figure 1, since (1) Hénon's results are based on Hill's approximation $\mu \to 0$, while the giant planets have μ in the range 0.00096 (Jupiter) to 0.000044 (Uranus); (2) Hénon's results assume that the planet orbit is circular, while the giant planets have eccentricities between 0.0086 and 0.056; (3) both the satellites and their host planets are subject to perturbations from the other planets. We must carry out long-term numerical integrations of the satellite orbits to assess the influence of these effects on the stability region shown in Figure 1.

We sample the initial conditions using a fine grid on the Hénon diagram, with $d\Gamma = 0.1$ and $d\xi = 0.06$. This is shown as the dotted grid in Figure 2. We then convert them to the nonrotating (xyz) planetocentric coordinate system where we do the integrations of satellite orbits. We require that in the rotating frame the Sun is always located at the $-\xi$ axis, and the angular velocity of the rotating frame equals the instantaneous angular velocity of the Sun relative to the planet in the nonrotating planetocentric frame; thus the angular speed of the rotating frame is time-varying if the planet's orbit is eccentric, and the direction of the ζ axis may vary if the planet's orbit is perturbed by other planets. We use a unit of length $\mu^{1/3} a_p$ and unit of time n^{-1} to scale the coordinates/velocities between the two frames, where a_p is taken to be the initial semimajor axis of the planet.

The system to be numerically integrated is composed of the four outer giant planets (or sometimes just one of them), the Sun, and a satellite around one of the planets; the satellite is treated as a massless test particle. We use a second-order Wisdom–Holman symplectic scheme (Wisdom & Holman 1991), as implemented in the SWIFT software package (Levison & Duncan 1994). Following Nesvorný et al. (2003), we have modified the SWIFT code such that the integration of the planets is done in the Jacobi coordinate system, while that of the satellites is done in the nonrotating planetocentric coordinate system. We tried different timesteps to optimize between speed and accuracy, and found $dt = 20$ days is short enough to produce the correct results with reasonable computational cost, for all four planets.

One potential concern is that the Wisdom–Holman symplectic scheme, as we have implemented it, is designed for nearly

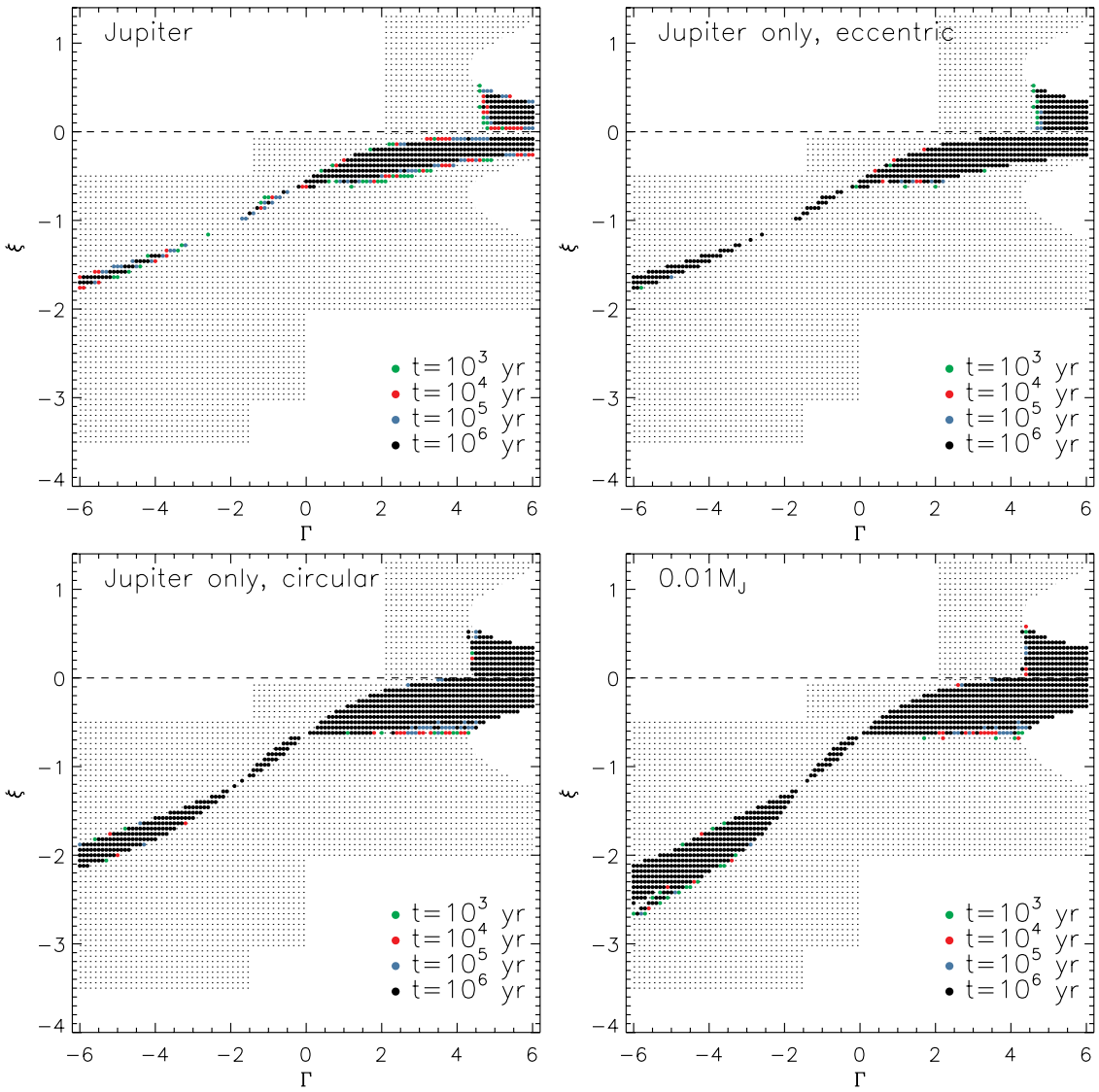

Figure 2. Hénon diagrams for Jupiter under various circumstances (see Section 3.1 for details). The satellite orbital plane initially coincides with Jupiter's. In each panel, the dotted region is the grid of initial conditions in the (Γ, ξ) plane. The two blank regions in the upper-right corner are forbidden. The filled circles in different colors represent the initial conditions of orbits that survive for various times.

(A color version of this figure is available in the online journal.)

Keplerian orbits relative to the planet and might break down at large distances from the planet, where the orbits are nearly Keplerian relative to the Sun. However, the characteristic orbital period at large distances is equal to the planetary orbital period, and this is much longer than the orbital periods of satellites inside the Hill radius that the integrator is designed to follow, so even a crude integrator should work well. Moreover, our ability to reproduce the Hénon diagram (compare Figure 1 and the lower right panel of Figure 2), the long-term stability of many of our orbits, and the similarity of the characteristic orbit shapes to those found by Hénon (see Section 3.1), all indicate that, even at the largest distances probed here, the symplectic integrator seems to work pretty well. As a further check, we have used the Bulirsch–Stoer integrator to follow satellite orbits around Uranus for 10^6 yr and found almost identical results to the Wisdom–Holman integrator.

We terminate the integration if the distance of the satellite from the planet exceeds the semimajor axis of the planet since at this point the satellite has escaped according to our definition at the end of Section 1, or if the distance is less than the semimajor axis of the outermost regular satellite of each planet (being Callisto, Iapetus, Oberon and Triton respectively), since at this point the satellite lifetime against ejection or collision with the regular satellite or the planet is likely to be short. Any test particles that cross either of these two radii are considered lost. We have experimented with including the quadrupole moment J_2 of the planet (including the contribution from the inner regular satellites), but this has no detectable effect on our results.

3. RESULTS

3.1. Two-Dimensional Hénon Diagrams

We first study cases in which the initial velocity vectors of satellites lie in the planet orbital plane, i.e., $\zeta = \dot{\zeta} = 0$. As we have described, this is different from Hénon's problem (Hénon 1970) because (1) we do not use Hill's approximation, (2) planets such as Jupiter have nonzero eccentricity, and (3) there are gravitational perturbations from other planets.

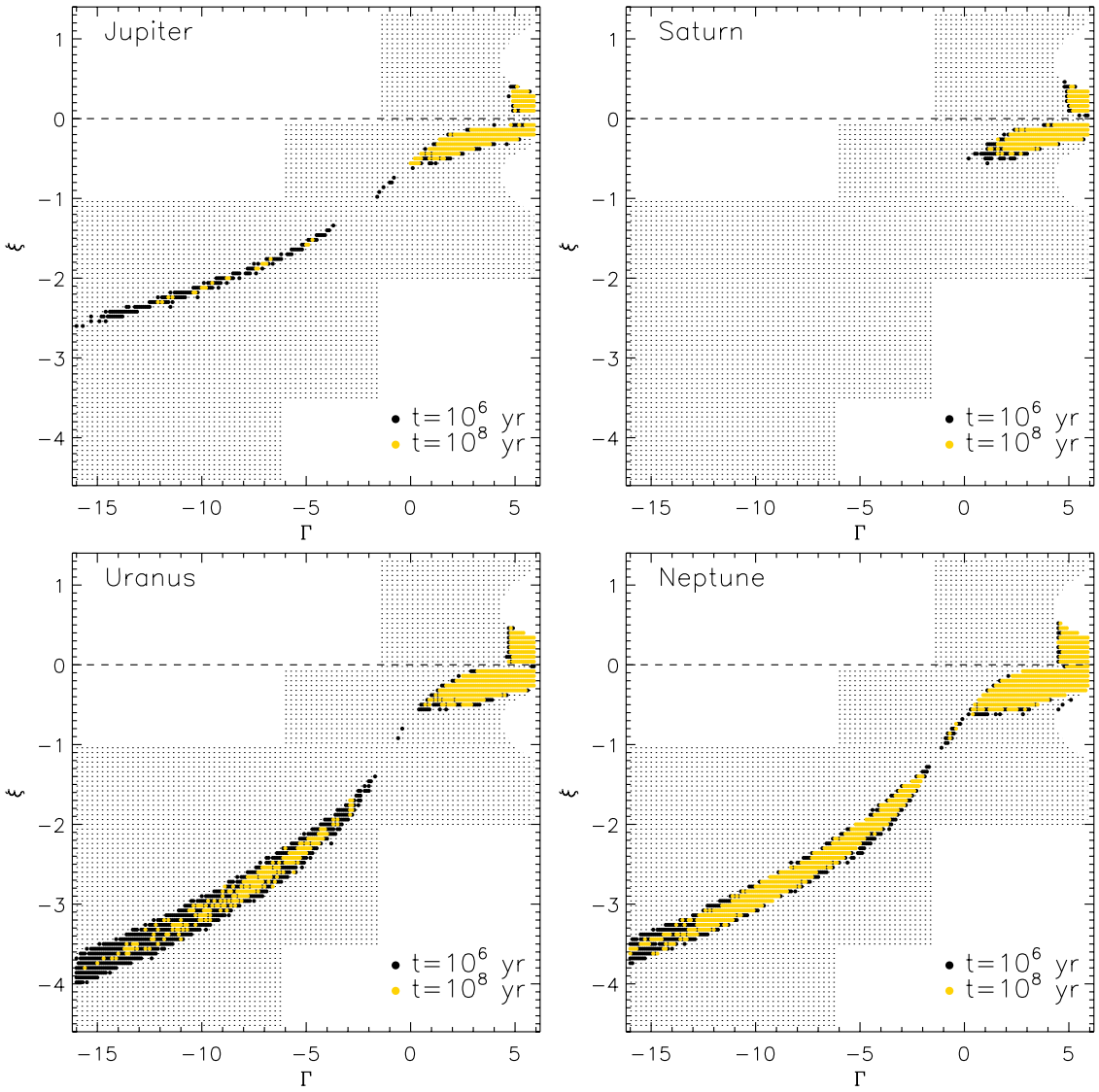

Figure 3. Two-dimensional Hénon diagrams for the four planets. Each orbit is integrated up to 10^8 yr under the gravitational influence of its host planet, the Sun, and the other three giant planets. Notations are the same as in Figure 2.

(A color version of this figure is available in the online journal.)

As an illustration we show how the stable region changes under various conditions in Figure 2, for satellites around Jupiter and an integration time of 10^6 yr. We consider four situations: (1) Jupiter moves on its actual (slightly eccentric) orbit, including perturbations from the other three giant planets (upper left); (2) the planar restricted three-body problem, in which Jupiter travels on an orbit with its current eccentricity of 0.048 and the other planets are absent (upper right); (3) the planar circular restricted three-body problem, in which Jupiter travels on a circular orbit with its current semimajor axis (bottom left); (4) the same as (3) except that the planet mass is 1/100 of the Jupiter mass (bottom right).

By comparing Figures 1 and 2 it is clear that case (d) in the bottom right panel best reproduces the original Hénon diagram; this is not surprising since $\mu \simeq 10^{-5}$ is smallest so Hill's approximation is satisfied best, and the other conditions assumed in Hénon's (1970) problem (circular planet orbit, no other planets) are also satisfied. When using the actual Jupiter mass in (3), the outer retrograde stable region (i.e., the lower-left branch) shifts and shrinks. The overall stability region shrinks further—but does not vanish—when Jupiter's orbit is eccentric as in case (2), and for the most realistic case (1).

Note that 10^6 yr is only a small fraction of the lifetime of the solar system, and possible erosion of the stable region over longer times is somewhat indicated by the presence of a few red and blue dots in the upper panels of Figure 2, indicating orbits that are unstable on timescales of 10^4 and 10^5 yr.

These illustrative calculations show that some Jovian satellites orbiting well outside the Hill radius can survive for at least 10^6 yr, although the stable region is substantially smaller than in Hill's approximation to the circular restricted three-body problem and appears to erode slowly with time. They also show that the stable region is larger (relative to the Hill radius) if the planet mass μ is smaller, suggesting that the stable regions of the other giant planets may be larger than Jupiter's.

We now extend these calculations in the following ways: (1) we examine satellite orbits around all four giant planets, using the actual planetary orbits including perturbations from

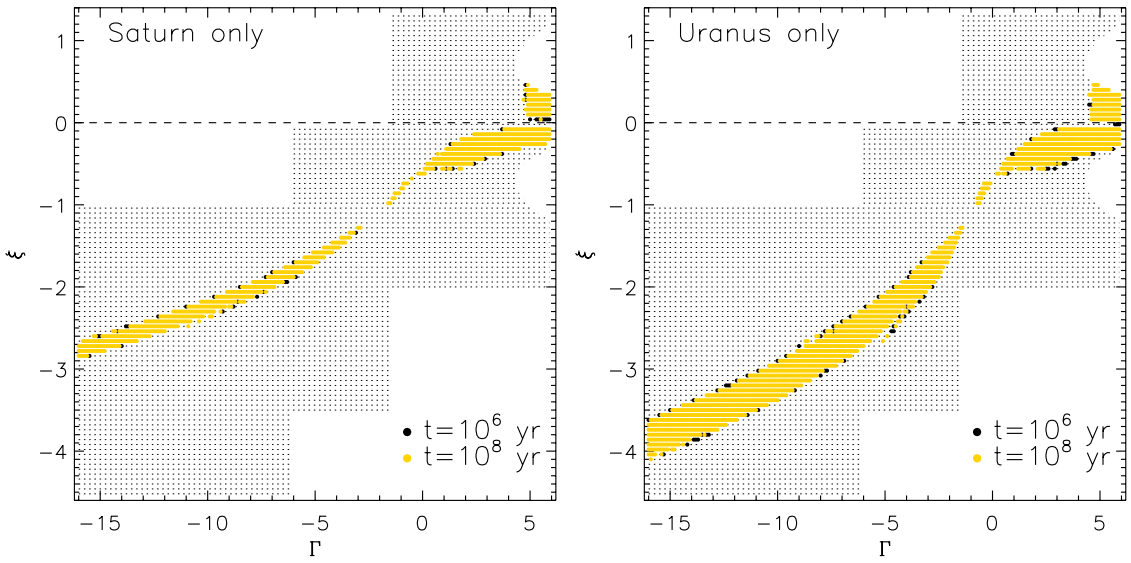

Figure 4. Two-dimensional Hénon diagrams for Saturn only (left) and Uranus only (right); the effects of the other three planets are not included in the integrations. In contrast to the results in Figure 3, Saturn can host stable outer retrograde orbits, and most of the satellites that survive for 10^6 yr also survive for 10^8 yr around both planets.

(A color version of this figure is available in the online journal.)

the three other planets; (2) since stable orbits are found at the most negative Jacobi constant ($\Gamma = -6$) examined in Figure 2, we extend the grid of initial conditions to $\Gamma = -16$; (3) we extend the integration time from 10^6 yr to 10^8 yr.

The results are shown in Figure 3. There are large regions of inner retrograde/prograde orbits that are stable for 10^8 yr. For Jupiter, there are a few outer retrograde orbits that survive for 10^8 yr; Wiegert et al. (2000) found no orbits that survived for $\gtrsim 10^7$ yr, but this may reflect their less complete coverage of phase space. For Saturn, the outer retrograde stable region completely disappears in less than 10^6 yr, a conclusion already reached by Wiegert et al. For Uranus and Neptune, in contrast, there is a large stable region of outer retrograde orbits remaining after 10^8 yr. We expect that the stable regions around Jupiter, Uranus, and Neptune will shrink somewhat further between 10^8 yr and 5×10^9 yr, the approximate age of the solar system, so we integrated some outer retrograde satellite orbits around these three planets for 10^9 yr. We found that about a third of the Jovian orbits and over half of the outer retrograde orbits for Uranus and Neptune shown in Figure 3 still survive. Thus it is very likely that Uranus and Neptune could still host primordial satellites on such orbits to the present time. It is likely, but not certain, that similar satellites could survive around Jupiter, at least in small volumes of phase space.

The shrinkage of the stable region of the outer retrograde branch between 10^6 and 10^8 yr, as well as the lack of stable outer retrograde orbits around Saturn, appear to be mainly due to perturbations from the other planets. To demonstrate this, we ran two 10^8 yr integrations for Saturn only and Uranus only. The results are shown in Figure 4; in this case, Saturn *can* host stable outer retrograde satellites for at least 10^8 yr, and there is almost no difference in the size of the stable region between 10^6 and 10^8 yr for either planet.

The stable region around Uranus is larger than the one around Saturn in Figure 4, and the stable regions around Uranus and Neptune are larger than the one around Jupiter in Figure 3. These differences are probably caused mostly by their different planet-to-Sun mass ratios μ. As μ increases, the outer retrograde stability branch in the lower left of the Hénon diagram shrinks, and shifts upward (see Hénon 1965; 1970; or compare the two lower panels of Figure 2).

We also notice that in Figure 2(d) and in the right panel of Figure 4 there is a little tail or branch to the stable region around $(\Gamma, \xi) = (-5, -2.5)$. We suspect this comes from Hénon's periodic family g_3 (Hénon 1969), which bifurcates from the periodic retrograde orbits at $(\Gamma, \xi) = (-2, -1.2)$ and passes close to the point $(\Gamma, \xi) = (-5, -2.5)$ (see Hénon 1970, Figure 13).

What do these stable orbits look like? In Hill's approximation, the stable (outer and inner) retrograde and inner prograde orbits are generated from the periodic f and g families respectively using the terminology of Hénon (1969). We show examples of stable orbits (i.e., those that survived for 10^8 yr) around Uranus in Figure 5. For each example orbit, we plot the instantaneous locations for the first one million years as dots with the two stars marking the starting and ending locations. We also plot the trajectory for several revolutions. Each orbit is plotted in both the nonrotating planetocentric x–y plane (left column) and the rotating ξ–η plane (right column). In the rotating frame, the inner prograde orbit (top panel) is elongated along the Sun–planet axis while the inner retrograde orbit (middle panel) is elongated perpendicular to the Sun–planet axis. The outer retrograde orbit (bottom panel) is also elongated perpendicular to the Sun–planet axis and oscillates about the planet as an ellipse with an axis ratio of approximately 2:1 (compare Figure 11 of Hénon 1970), as one would expect from epicycle theory.

Note that the stable retrograde orbits with ξ close to -0.6934 in Figure 3 regularly cross the Hill radius. Hence such orbits are missed by the surveys of both Wiegert et al. (2000) and Nesvorný et al. (2003), who terminate their integrations if $r < r_H$ or $r > r_H$, respectively.

3.2. Three-Dimensional Hénon Diagrams

We now extend the initial conditions in Section 3.1 to three dimensions by including the scaled vertical coordinate ζ. As

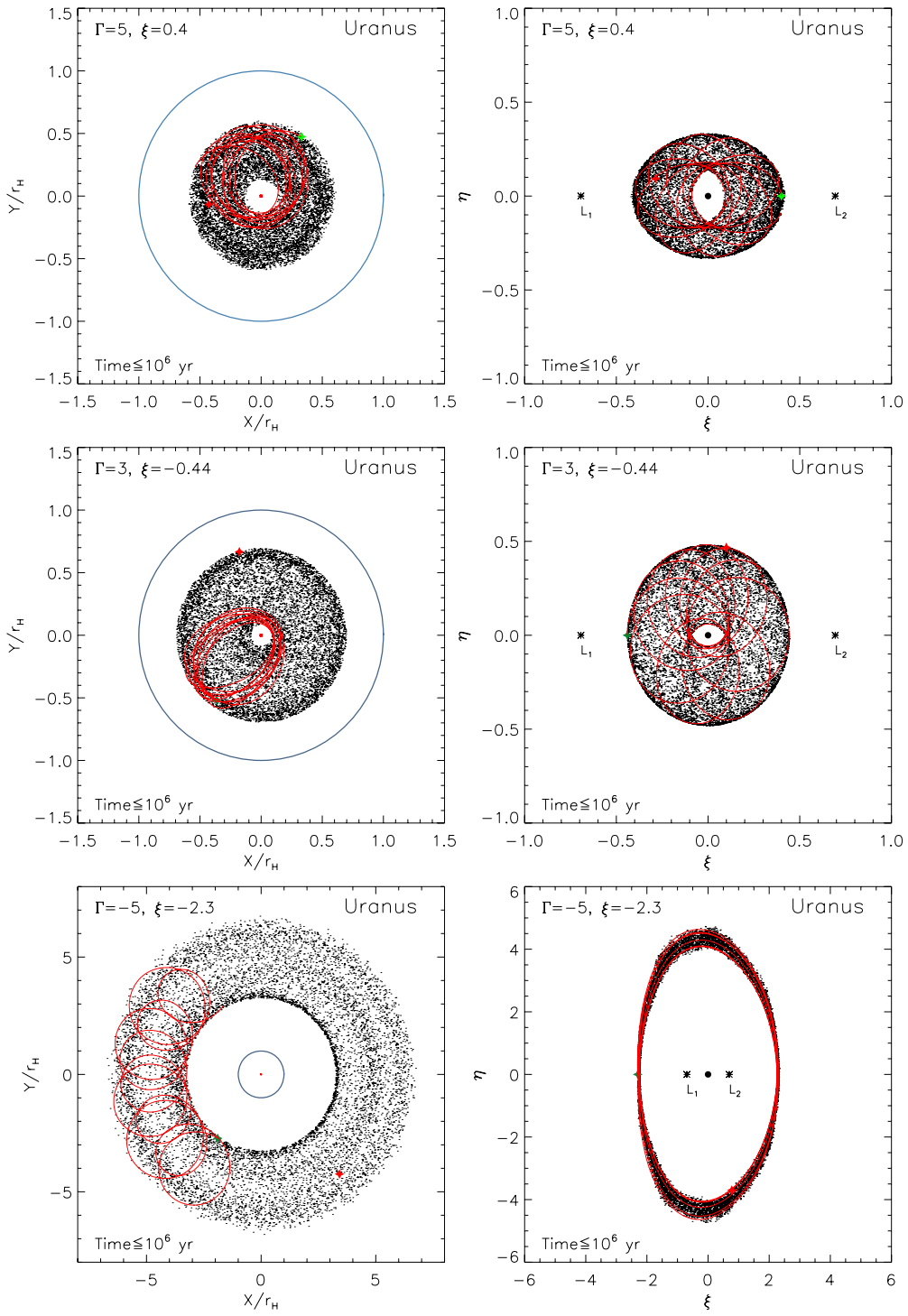

Figure 5. Examples of stable orbits around Uranus. All orbits initially lie in the orbital plane of Uranus. Dots are instantaneous locations for the first 10^6 yr, plotted at intervals of 100 yr, with the green and red stars marking the starting and ending locations. We also plot a few revolutions as red curves. The left column is in the *nonrotating* planetocentric frame and the right column is in the *rotating* planetocentric frame. In the left column, the blue circles indicate the Hill sphere. Upper: an inner prograde orbit; middle: an inner retrograde orbit; bottom: an outer retrograde orbit.

(A color version of this figure is available in the online journal.)

discussed in Section 2.1, we consider a surface of section $\eta = \zeta = \dot{\xi} = 0$, $\dot{\eta} > 0$ at $t = 0$. Similar to the two-dimensional case, we sample the initial conditions using a fine grid in the (Γ, ξ) plane, and use Equation (9) to generate initial velocities. We choose a sequence of inclinations in the rotating frame, $I = 15°, 30°, 45°, 60°, 75°$. Each satellite orbit is then integrated for 10^8 yr along with the four giant planets and the Sun.

The general behavior when incorporating inclination is the erosion of stable regions in the Hénon diagram. As an example, we show the results for Uranus in Figure 6. The outer retrograde orbits quickly become unstable when the initial inclination exceeds $\approx 20°$. The inner retrograde stable region erodes with increasing inclination and disappears at $I \gtrsim 75°$. The inner prograde stable region can survive even at $I \approx 75°$. This asymmetry between inner retrograde and prograde orbits is due,

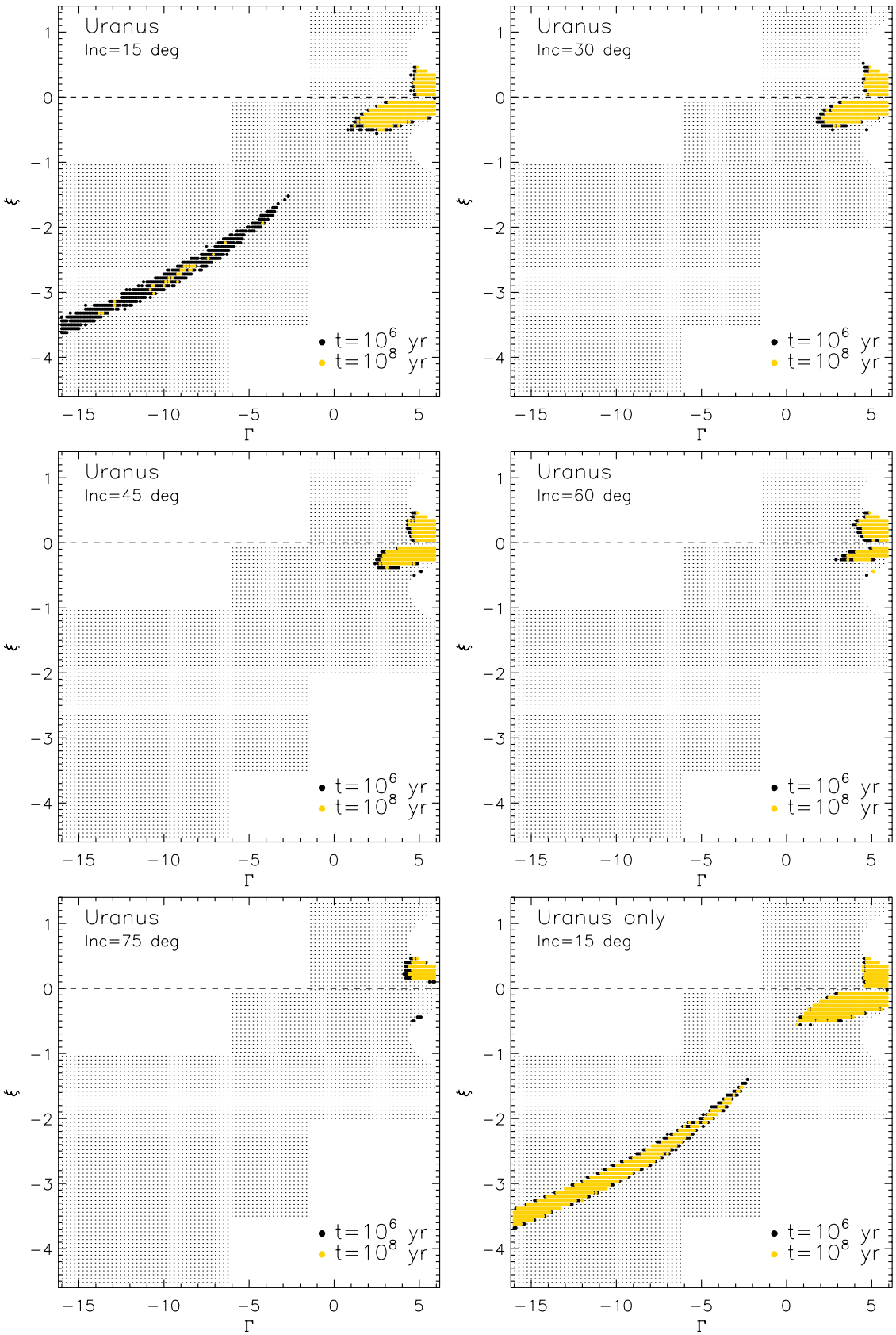

Figure 6. Examples of three-dimensional Hénon diagrams for Uranus. The initial inclinations $I = 15°, 30°, 45°, 60°, 75°$ in the rotating frame. The notation is the same as in Figures 2 and 3. The stable regions shrink as the inclination increases. In particular, no stable outer retrograde orbit exists for $I \geqslant 30°$.

(A color version of this figure is available in the online journal.)

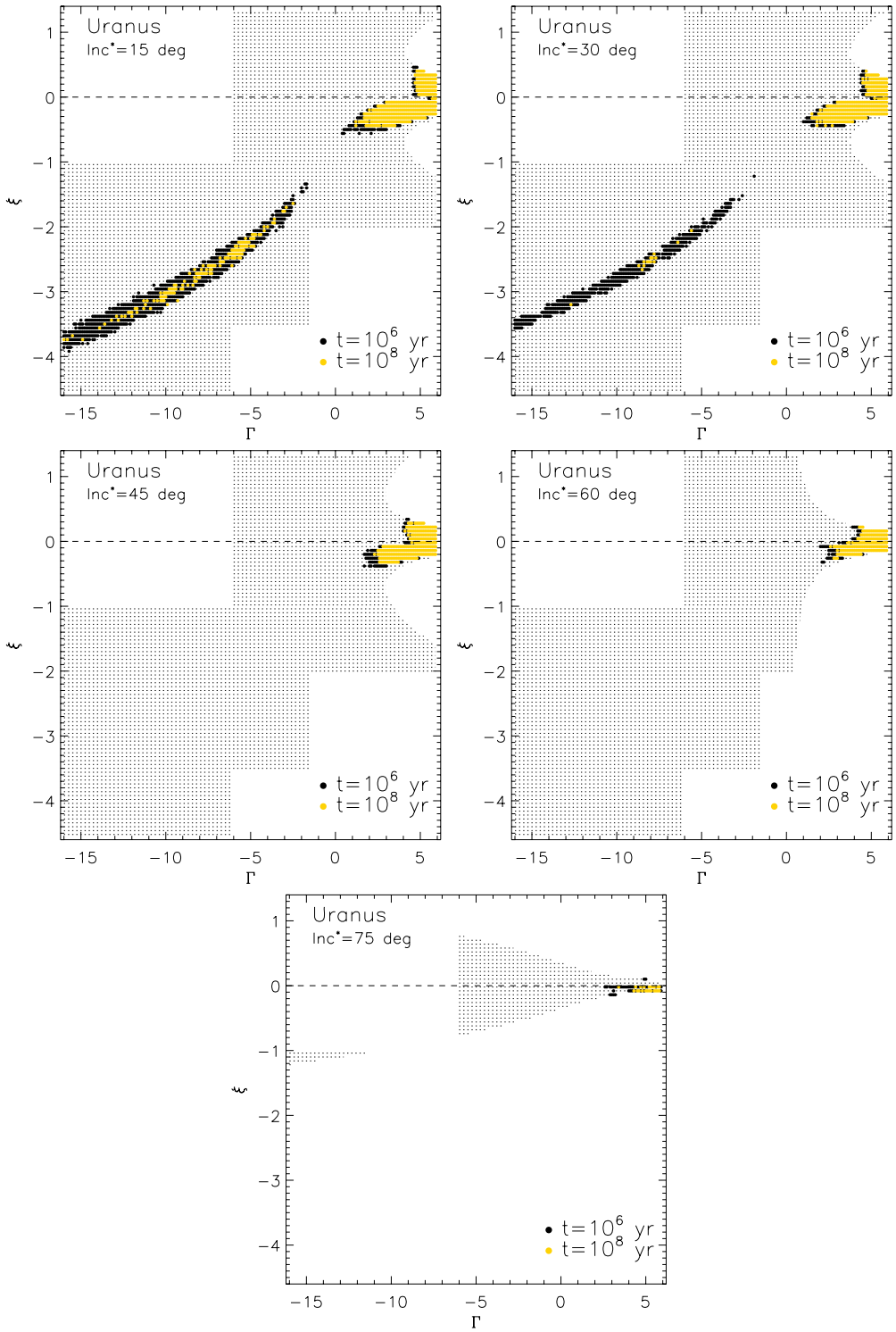

Figure 7. Examples of three-dimensional Hénon diagrams for Uranus. In these diagrams the surface of section is taken when the satellite is at maximum height above the planet's orbital plane (in contrast to Figure 6 where the surface of section is taken when the satellite crosses the plane). The initial inclinations $I^* = 15°, 30°, 45°, 60°, 75°$ in the rotating frame.

(A color version of this figure is available in the online journal.)

in part, to the definition of inclination in the rotating frame.[5] However, even when inclination is defined in the nonrotating frame such an asymmetry may still be present (see Ćuk & Burns 2004 for a discussion of the dynamical reasons for the asymmetry).

To separate the destabilizing effects of inclination from the effects of perturbations from other planets, we also ran these three-dimensional simulations for Uranus without the other

[5] When translated into the nonrotating planetocentric frame, the inclinations of "prograde" ("retrograde") orbits are actually smaller (larger) than in the rotating frame. As we already noted in Figure 1, under certain circumstances retrograde orbits in the rotating frame can even be prograde in the nonrotating frame.

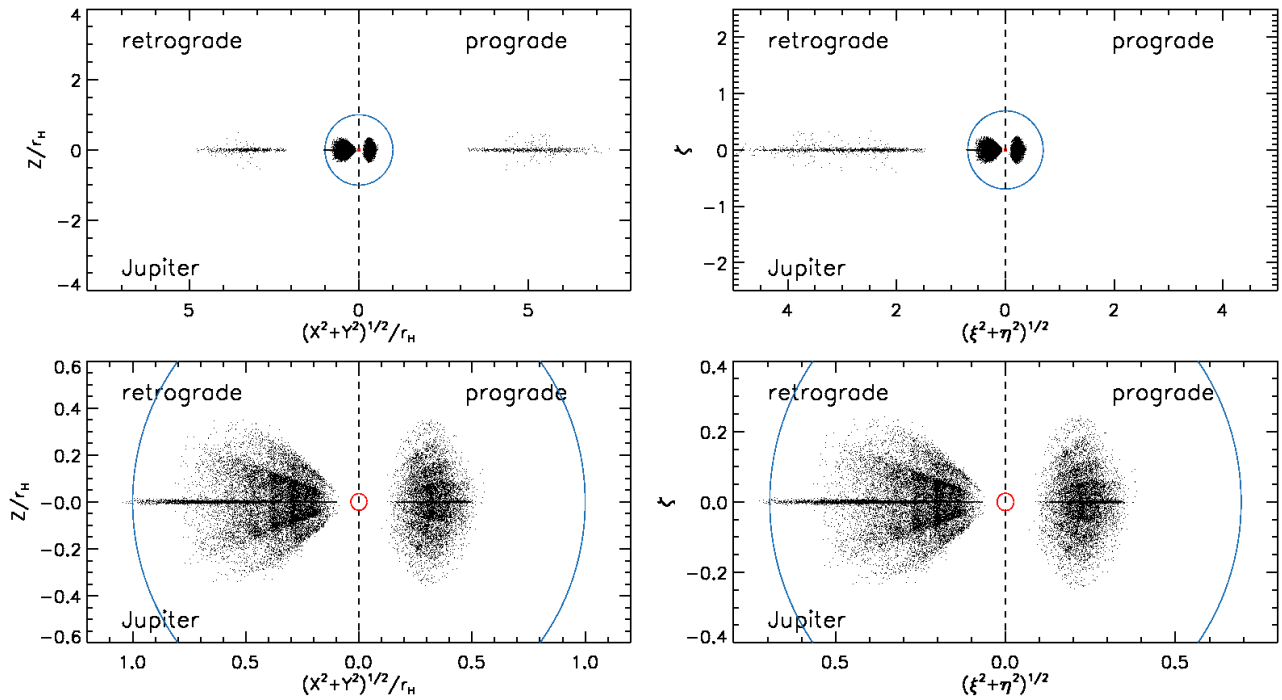

Figure 8. Spatially accessible regions of stable satellite orbits for Jupiter. The left column is in the *nonrotating* planetocentric frame and the right column is in the *rotating* planetocentric frame. The bottom two panels show expanded views of the inner portions of the upper two panels. In each panel, retrograde orbits and prograde orbits are plotted separately in the left and right halves, with "prograde/retrograde" defined in each frame used. The blue circles show the Hill sphere and the smaller central red circles show the inner boundary in the numerical integrations (the orbital radius of the outermost regular satellite, in this case Callisto). The extreme thinness of the zone of stable retrograde orbits outside the Hill sphere is an artifact of our simulations, which sampled the initial inclinations only at 0°, 15°, ...

(A color version of this figure is available in the online journal.)

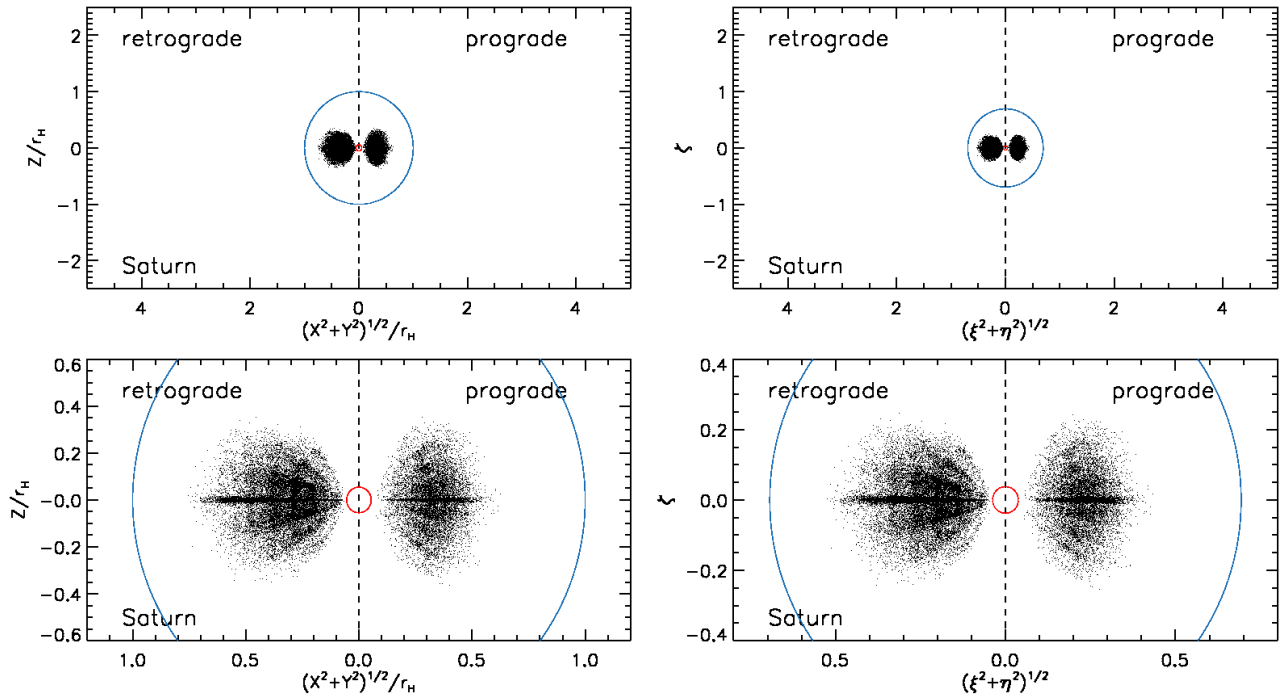

Figure 9. Spatially accessible regions of stable satellite orbits for Saturn. The notation is the same as in Figure 8.

(A color version of this figure is available in the online journal.)

planets. We found that for $I \lesssim 20°$, perturbations from other planets do play a major role in eroding the region of stable outer retrograde orbits, as illustrated by comparing the upper left and lower right panels of Figure 6, which show the Hénon diagram for $I = 15°$ with and without the other planets. However, for $I = 30°, 45°, 60°, 75°$ the results for Uranus alone are almost identical to the realistic case which includes perturbations from the three other planets. This result suggests that bound retrograde orbits outside the Hill sphere may not exist at all for $I \gtrsim 20°$. This is expected because the Coriolis

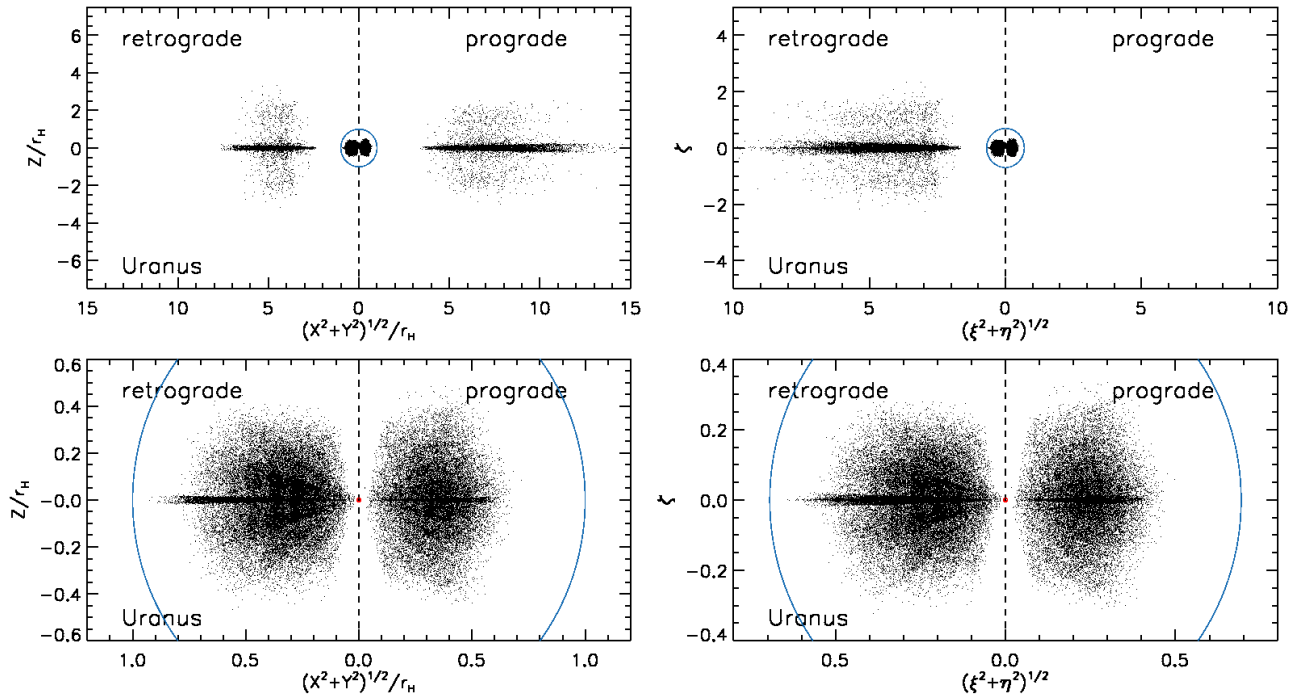

Figure 10. Spatially accessible regions of stable satellite orbits for Uranus. The notation is the same as in Figure 8.
(A color version of this figure is available in the online journal.)

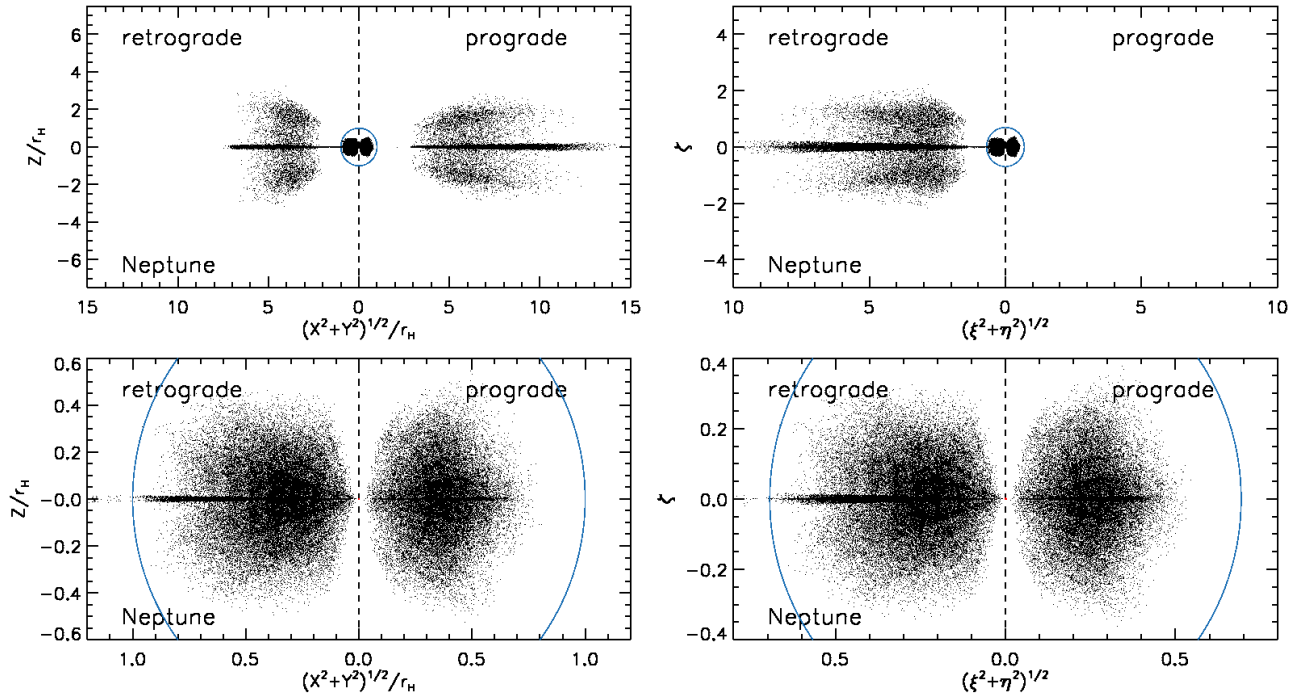

Figure 11. Spatially accessible regions of stable satellite orbits for Neptune. The notation is the same as in Figure 8.

force, which stabilizes outer retrograde orbits by bending their trajectory toward the planet in the rotating frame, is reduced when the inclination angle I increases. This shrinkage of the stable outer retrograde branch with inclination is already noticed by comparing the right panel of Figure 4 ($I = 0$) and the bottom-right panel of Figure 6 ($I = 15°$).

Note that the inclinations I are planetocentric and measured in the rotating frame. For low-inclination orbits along the outer retrograde branch they can be converted to heliocentric inclinations i using the approximate formula for small e

$$i \approx 2eI \ , \tag{10}$$

where e is the heliocentric eccentricity. Thus our stability region $I \lesssim 20°$ corresponds roughly to $i \lesssim 4°$ for $e \approx 0.1$, the typical heliocentric eccentricity of surviving satellites for Uranus and Neptune (see Figure 12); this is in reasonable agreement with the

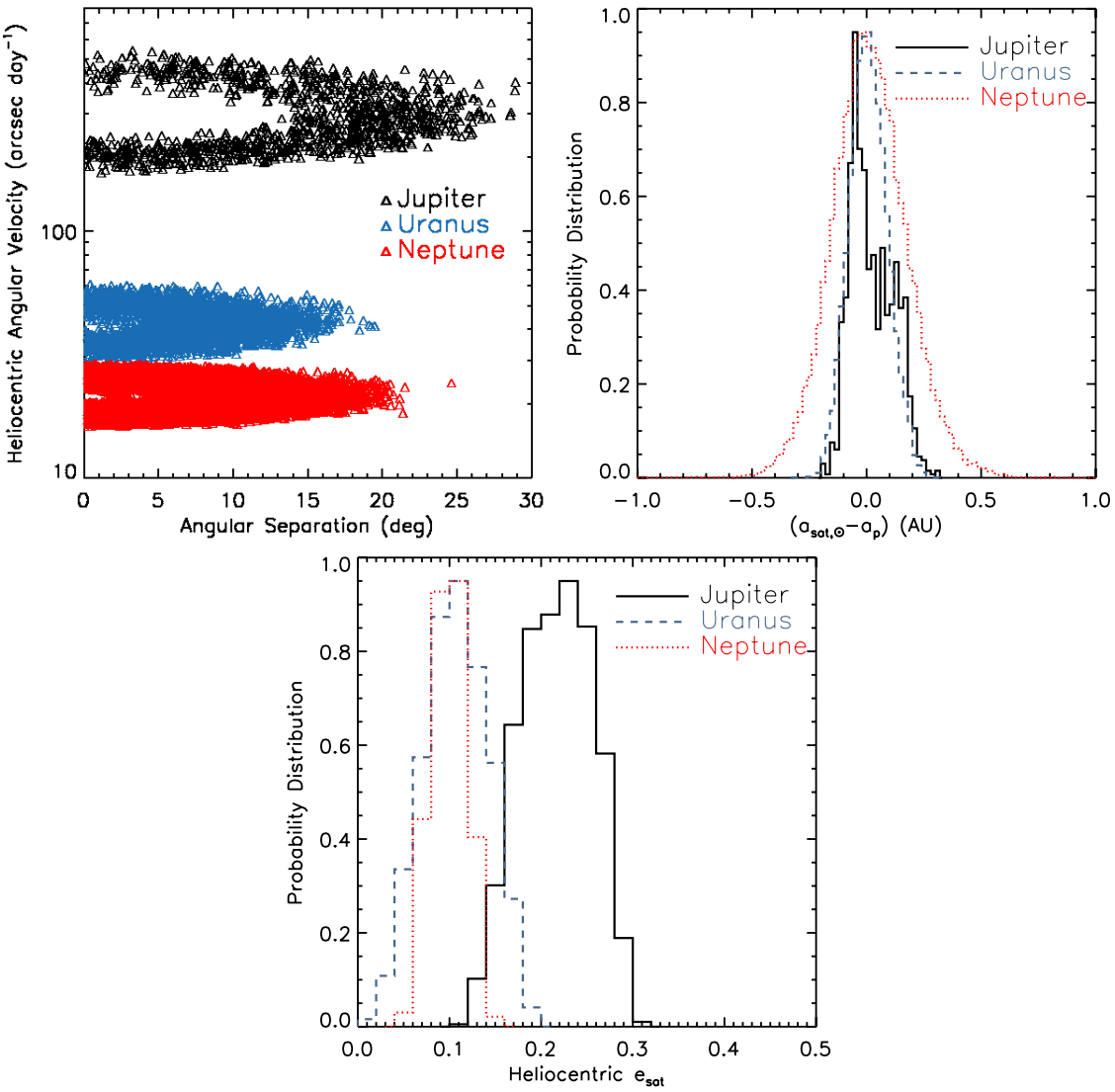

Figure 12. Upper left: heliocentric angular velocities of the stable outer irregular satellites as a function of angular distance from the planet, as viewed from the Sun in the nonrotating frame. Upper right: histograms of the difference between the heliocentric satellite semimajor axis and the planet semimajor axis for the stable outer irregular satellites, where the peaks of these distributions are arbitrarily scaled. Bottom: histograms of the heliocentric eccentricity for the stable outer irregular satellites. The sampling of points is the same as we used to produce the spatial stability regions in Section 3.3.

(A color version of this figure is available in the online journal.)

estimate of Wiegert et al. (2000) that most of their long-lived orbits had $i \lesssim 2°$, especially considering that our sampling of initial conditions is more complete than theirs. Mikkola & Innanen (1997) and Mikkola et al. (2006) estimate analytically that the outer retrograde orbits are unstable if $i > e$ (for a circular planet orbit), which implies instability if $I \gtrsim 30°$. Our own results show that all the test particles with initial positions outside the Hill sphere cross the escape radius a_p well before 10^4 yr for $I \geqslant 30°$.

As described at the end of Section 2.1, a limitation of these results is that the Hénon diagram we have used will not display orbits trapped in a Kozai resonance, or other stable orbits whose argument of pericenter does not periodically pass through 0 or π. To estimate the contribution of such orbits, we have constructed a different set of three-dimensional Hénon diagrams in which the initial conditions are changed from our usual choice $\eta = \dot{\xi} = \zeta = 0, \dot{\eta} > 0$ to $\eta = \dot{\xi} = \dot{\zeta} = 0, \dot{\eta} > 0$ (i.e., when the orbit is at its maximum height above the planet's orbital plane, rather than crossing the orbital plane). In this case, we define the initial inclination I^* in the rotating frame by

$$\tan I^* = \left.\frac{\zeta}{\xi}\right|_{t=0}. \tag{11}$$

The results are shown in Figure 7, which should be compared to Figure 6. Each point in either set of Hénon diagrams corresponds to a unique orbit, but orbits appearing in the Hénon diagrams of one figure at a given value of (Γ, ξ, I) may or may not appear in the other figure, where they will have the same value of Γ but possibly different values of ξ and inclination. The stable regions are somewhat larger in Figure 7 at a given inclination—for example, a few outer retrograde satellites survive for 10^8 yr at $I^* = 30°$—but the conclusions described above are not significantly altered. In the following discussion, we neglect stable orbits that do not appear in our fiducial Hénon diagrams (i.e., using the surface of section $\eta = \dot{\xi} = \zeta = 0, \dot{\eta} > 0$); thus

we may slightly underestimate the size of the stable regions. More discussion on orbits trapped in the Kozai resonance inside the Hill sphere can be found in Carruba et al. (2002).

3.3. Spatial Stability Regions

We now project the phase-space volume that hosts stable orbits onto coordinate space, to explore where stable satellites might be found.

We plot the positions of stable orbits in the two-dimensional plane with coordinates $\left[(x^2 + y^2)^{1/2}, z\right]$ (nonrotating frame) or $\left[(\xi^2 + \eta^2)^{1/2}, \zeta\right]$ (rotating frame). Prograde and retrograde orbits are plotted separately on the left and right sides of a given figure panel, where "prograde" and "retrograde" are defined in the frame used. We plot the position of each stable (up to 10^8 yr) point in the Hénon diagram at uniformly spaced times (every Myr) between 5×10^7 and 10^8 yr in Figures 8 (Jupiter) to 11 (Neptune).

The stability regions within the Hill sphere are very similar to those shown in Figures 9–12 of Nesvorný et al. (2003), though slightly larger because we show instantaneous position rather than semimajor axis. For Jupiter and Saturn, the stable prograde orbits generally extend to $\sim 0.5 r_{\rm H}$; the stable retrograde orbits can extend further to $\sim 0.7 r_{\rm H}$, and nearly coplanar retrograde orbits even extend to $\sim r_{\rm H}$ for Jupiter. For Uranus and Neptune, both the prograde and retrograde stable orbits can extend a little bit further relative to the Hill sphere. No stable orbits exist at high latitudes, presumably because of Kozai oscillations (Kozai 1962; Carruba et al. 2002; Nesvorný et al. 2003).

It is also notable that there are stable regions beyond the Hill sphere for Jupiter, Uranus and Neptune, as we discussed in previous sections. This is particularly the case for Uranus and Neptune. Most of these distant stable satellites are concentrated close to the orbital plane of the planet as for Jupiter, although the appearance of a very thin layer in Figures 8 (Jupiter) to 11 (Neptune) is somewhat an artifact of the coarse sampling of inclinations in our initial conditions ($I = 15^\circ, 30^\circ, 45^\circ, 60^\circ, 75^\circ$). Stable satellites can be found as far as $\sim 5 r_{\rm H}$ from Jupiter and even $\sim 10 r_{\rm H}$ for Uranus and Neptune, and as high as $2.5 r_{\rm H}$ above the orbital plane for the latter two planets. In the following section, we discuss briefly the strategy of searches for these distant satellites.

4. DISCUSSION AND CONCLUSIONS

We have conducted a systematic survey of the stable regions of satellites around giant planets in the solar system, using numerical orbital integrations that include gravitational perturbations from the other planets. We confirm previous results for satellites within the Hill sphere: stable retrograde satellites can exist further out than prograde satellites (e.g., Hénon 1970; Hamilton & Krivov 1997; Nesvorný et al. 2003); and stable orbits cannot exist at high inclinations (e.g., Carruba et al. 2002; Nesvorný et al. 2003).

We also confirm and extend the conclusions of Wiegert et al. (2000) that distant retrograde satellites ("retrograde" as defined in the rotating frame) can survive well beyond the Hill sphere for at least 10^8–10^9 yr, and probably for the lifetime of the solar system. Uranus and Neptune are the most promising host planets for such distant satellites, since their stability regions have the largest extent (e.g., Figures 10–11). Jupiter has a smaller stable region (Figure 8), and Saturn appears to have no stable regions beyond the Hill radius (Figure 9).

Remarkably, there is a gap between the inner and outer stability zones for retrograde satellites, extending from about $r_{\rm H}$ to $2r_{\rm H}$, in which almost no stable orbits exist.

To check whether any of the proposed distant satellites have already been discovered as Centaurs, we take the positions and velocities of the known Centaurs from the IAU Minor Planet Center[6] that have planetocentric distances smaller than the semimajor axes of each of the four giant planets at the last observed epoch. There are 31 Centaurs (Jupiter 1; Uranus 16; Neptune 14) that satisfy the criterion. We numerically integrated these objects along with the Sun and giant planets for 10^8 yr, but none of them survived as satellites according to the definition in Section 1.

Searches for satellites far beyond the Hill radius can be carried out either with dedicated deep, wide-angle surveys around the giant planets, or through all-sky surveys such as the Panoramic Survey Telescope and Rapid Response System and the Large Synoptic Survey Telescope. The most promising search areas are close to the orbital plane of the planet, since only low-inclination orbits survive (e.g., compare Figure 3 and Figure 6). In Figure 12 (upper left panel) we show the heliocentric angular velocity of the stable outer retrograde satellites as a function of angular distance from the planet as viewed from the Sun, for Jupiter (black), Uranus (blue), and Neptune (red) respectively, sampled every Myr between 5×10^7 and 10^8 yr.

In the upper right and bottom panels of Figure 12, we show histograms of the difference in heliocentric semimajor axis from their host planet and heliocentric eccentricities for the stable outer retrograde satellites. These distributions can be used to cull a large sample for potential satellites. Once a candidate is identified with reliable orbit elements, a long-term orbital integration should be run to confirm its satellite nature.

The discovery and characterization of satellites beyond the Hill sphere would provide rich information about the early formation of the solar system. Fabrycky (2008; also see, Kortenkamp 2005) recently performed simulations of capture of neighboring planetesimals from the circumstellar disk during slow planet growth, and found that such distant satellites are a natural outcome for Uranus and Neptune. Thus an inventory of this potential population of bodies would enhance our understanding of the formation of planets and their satellites in the early solar system, and the properties of the primordial planetesimal disk.

This research was supported in part by NASA grant NNX08AH83G. We thank Dan Fabrycky and the anonymous referee for comments that greatly improved the paper.

REFERENCES

Benest, D. 1971, A&A, 13, 157
Burns, J. A. 1986, in Satellites, ed. J. A. Burns & M. S. Matthews (Tucson, AZ: Univ. of Arizona Press), 1
Carruba, V., Burns, J. A., Nicholson, P. D., & Gladman, B. J. 2002, Icarus, 158, 434
Connors, M., et al. 2004, Meteorit. Planet. Sci., 39, 1251
Ćuk, M., & Burns, J. A. 2004, AJ, 128, 2518
Fabrycky, D. 2008, Icarus, submitted
Gladman, B. J., Nicholson, P. D., Burns, J. A., Kavelaars, J J, Marsden, B. G., Williams, G. V., & Offutt, W. B. 1998, Nature, 392, 897
Gladman, B., Kavelaars, J J, Holman, M., Petit, J. -M., Scholl, H., Nicholson, P., & Burns, J. A. 2000, Icarus 147, 320 (erratum in Icarus, 148, 320)
Gladman, B., et al. 2001, Nature, 412, 163

[6] http://cfa-www.harvard.edu/iau/mpc.html

Goldreich, P. 1966, Rev. Geophys. Space Phys., 4, 411
Hamilton, D. P., & Krivov, A. V. 1997, Icarus, 128, 241
Hénon, M. 1965, Ann. Astron., 28, 992
Hénon, M. 1969, A&A, 1, 223
Hénon, M. 1970, A&A, 9, 24
Hénon, M. 1974, A&A, 30, 317
Hill, G. W. 1886, Acta Math., 8, 1
Holman, M. J., et al. 2004, Nature, 430, 865
Jackson, J. 1913, MNRAS, 74, 62
Jewitt, D., & Haghighipour, N. 2007, ARA&A, 45, 261
Kavelaars, J. J., et al. 2004, Icarus, 169, 474
Kortenkamp, S. J. 2005, Icarus, 175, 409
Kozai, Y. 1962, AJ, 67, 591
Levison, H. F., & Duncan, M. J. 1994, Icarus, 108, 18
Lidov, M. L., & Vashkov'yak, M. A. 1994a, Astron. Lett., 20, 188
Lidov, M. L., & Vashkov'yak, M. A. 1994b, Astron. Lett., 20, 676
Mikkola, S., & Innanen, K. 1997, in The Dynamical Behaviour of our Planetary System, ed. R. Dvorak & J. Henrard (Dordrecht: Kluwer), 345
Mikkola, S., Innanen, K., Wiegert, P., Connors, M., & Brasser, R. 2006, MNRAS, 369, 15
Murray, C. D., & Dermott, S. F. 1999, Solar Systam Dynamics (Cambridge: Cambridge Univ. Press)
Namouni, F. 1999, Icarus, 137, 293
Nesvorný, D., Alvarellos, J. L. A., Dones, L., & Levison, H. F. 2003, AJ, 126, 398
Sheppard, S. S., & Jewitt, D. 2003, Nature, 423, 261
Sheppard, S. S., Jewitt, D., & Kleyna, J. 2005, AJ, 129, 518
Sheppard, S. S., Jewitt, D., & Kleyna, J. 2006, AJ, 132, 171
Wiegert, P., Innanen, K., & Mikkola, S. 2000, AJ, 119, 1978
Wisdom, J., & Holman, M. 1991, AJ, 102, 1528